Earthq Eng & Eng Vib (2023) 22: 157-172 **DOI**: https://doi.org/10.1007/s11803-023-2151-6

Triaxial elastoplastic damage constitutive model of unreinforced clay brick masonry wall

Wu Biye[1, 2†], Dai Junwu[1, 2‡], Bai Wen[1, 2§] and Yang Yongqiang[1, 2‡]

1. *Key Laboratory of Earthquake Engineering and Engineering Vibration, Institute of Engineering Mechanics, China Earthquake Administration, Harbin 150080, China*
2. *Key Laboratory of Earthquake Disaster Mitigation, Ministry of Emergency Management, Harbin 150080, China*

Abstract: Due to differences in the properties of composition materials and construction techniques, unreinforced masonry is characterized by low strength, anisotropy, nonuniformity, and low ductility. In order to accurately simulate the mechanical behavior of unreinforced brick masonry walls under static and dynamic loads, a new elastoplastic damage constitutive model was proposed and the corresponding subroutine was developed based on the concrete material constitutive model. In the proposed constitutive model, the Rankine strength theory and the Drucker-Prager strength theory were used to define the tensile and compressive yield surface function of materials, respectively. Moreover, the stress updating algorithm was modified to consider the tensile plastic permanent deformation of masonry materials. To verify the accuracy of the proposed constitutive model, numerical simulations of the brick masonry under monotonic and cyclic uniaxial tension and compression loads were carried out. Comparisons among the numerical and theoretical and experimental results show that the proposed model can properly reflect the masonry material mechanical properties. Furthermore, the numerical models of four pieces of masonry walls with different mortar strengths were established. Low cyclic loadings were applied and the results show that the proposed constitutive model can properly simulate the wall shear failure characteristics, and the force-displacement hysteretic curves obtained by numerical simulation are in good agreement with the tests. Overall, the proposed elastic-plastic damage constitutive model can simulate the nonlinear behavior of unreinforced brick masonry walls very well, and can be used to predict the structural response of masonry walls.

Keywords: brick masonry; elastoplastic model; calibration parameters; numerical simulation; damage variable

1 Introduction

Brick masonry structures have a long history due to cost-efficiency, easily accessible raw materials, and simple construction operation. They are widely used in residential, medical, and educational buildings. Statistics show that 40% to 50% of the world′s buildings are brick masonry structures. A study on seismic damage showed that the damage potential of masonry structures is particularly prominent when compared to others. Thus, the seismic safety of masonry structures has become a common concern in the civil engineering field (Sun and Zhang, 2018). Since the 1960s, structural tests have been an important part of research on the aseismic theory of masonry structures (Sachin *et al*., 2020; Ge *et al*., 2021). Scholars have conducted relevant experimental studies on these structures from different perspectives. However, the development of finite element analysis theory of masonry structures has been relatively slow. This is due to the complex material composition of masonry structure, which makes it difficult to accurately establish a reasonable analysis model.

In recent decades, scholars have carried out a lot of exploration and research work on masonry structures with different finite element calculation methods in pursuit of the unified goal of calculation accuracy and calculation efficiency. According to the different analysis scales (Lourenço, 2009; Roca *et al*., 2010; Addessi *et al*., 2014), these calculation methods can be divided into five strategies: micromechanical, mesoscale, multi-scale, discrete element and macro-mechanical method. The micromechanical method models the mortar and block of the wall in detail and selects the appropriate material model, and the interaction between the mortar

Correspondence to: Bai Wen, Institute of Engineering Mechanics, China Earthquake Administration, 9 Xuefu Road, Harbin 150080, China
Tel: +86-451-86652883
E-mail: baiwen@iem.ac.cn
†Professor of Engineering; ‡Professor; §Associate Professor

Supported by: National Key Research and Development Program of China under Grant Nos. 2018YFC1504400 and 2019YFC1509301, Natural Science Foundation of China under Grant No. 52078471, and Scientific Research Fund of Institute of Engineering Mechanics, China Earthquake Administration under Grant No. 2019EEEVL0402
Received July 6, 2020; **Accepted** April 12, 2021

and block is simulated through the face to face contact. This contact is considered as a potential fracture and slip surface that can simulate the nonlinear behavior of the masonry, including all possible failure mechanisms. The micromechanical method has fine mesh division and accurate calculation results, but it needs large-scale calculation resources, so it is mainly applicable to the analysis of masonry units, and is rarely used in the analysis of complete structures. (Agüera *et al*., 2016). The Mesoscale mechanical method is also called the micro interface element method. This method is an improvement to the micromechanical method; in this method, a block can be assumed as an elastic unit or rigid body, mortar is assumed to be a zero thickness interfacial contact unit, and all nonlinear behavior of the model (including tensile, shear and slip and compressive failure) are defined in the interface unit. This method can effectively save computing workload, and has been used by many scholars. (Lotfi and Shing, 1997; Lourenco and Rots, 1997; Oliveira and Lourenco, 2004; Sacco and Toti, 2010; Macorini and Izzuddin, 2011; Aref and Dolatshahi, 2013).

Multiscale modeling can be regarded as an intermediate method between macro modeling and micro modeling (Massart *et al*., 2010; Bellis and Addessi, 2011; Addessi and Sacco, 2012; Petracca, 2016). This method splits the component in length scale and establishes weak coupling. The microstructural features are inserted into a so-called equivalent volume unit (RVE), which is then used as a typical sample of the microstructure to obtain the homogeneous response of the macroscopic strain field to simulate the equivalent homogeneous medium. The model splits the structural problem into two scales: an equivalent homogeneous medium is studied on macro level, where the constitutive response at each material point is derived by homogenizing the stress fields computed in a properly selected representative volume element at the microscale; this last contains the detailed description of the masonry components geometry, arrangement and constitutive behavior and is analyzed at the microlevel. This method is used to solve linear and nonlinear problems with complex microstructure. In recent years, the discrete element method has been widely used as a new method in seismic assessment of masonry structures. In this method, the masonry materials are regarded as a collection of block units, which are held together by the interaction of the contact surfaces between the blocks, which is equivalent to the bonding effect of the masonry mortar, and the blocks can be a rigid body and an elastic body. This method has high computational efficiency and is widely used in seismic assessment and structural safety analysis (Schlegel and Rautenstrauch, 2004; Lemos, 2007; Bretas *et al*., 2014; Galvez *et al*., 2018; Sarhosis and Lemos, 2018).

In order to reduce the calculated amount and save computing time, a large number of scholars established a macro-mechanical model (Addessi *et al*., 2002; Berto *et al*., 2002; Karapitta *et al*., 2011; Abo-El-Ezz *et al*., 2013; Toti *et al*., 2015). In this method, the masonry structure is regarded as equivalent homogeneous anisotropic materials, and the mortar and block composition materials are no longer distinguished. Although it is difficult to establish the homogeneous constitutive model of masonry structures due to the differences in composition materials and construction technology, the macro-mechanical model is widely used to analyze the real complex structure, because it achieves a reasonable balance between calculation accuracy and calculation efficiency.

When the macro-mechanical method is applied to the analysis of masonry structures, it is mainly used for the seismic analysis of the whole structure. Few scholars have applied this method to simulate the masonry wall components, because it is a challenge for the macro-mechanical method to reproduce the wall failure characteristics and the bearing capacity degradation mechanism. In this research, the macro-mechanical method is used to study the cyclic response of masonry wall components under the action of quasi-static force. The masonry elasto-plastic damage material model subroutine is developed under the LS-DYNA platform.

The numerical simulation methods used in other materials (such as concrete, rock, and composite materials) are not applicable in the static and dynamic analyses of masonry structures due to their special anisotropic properties. Therefore, the research and development of the constitutive model of anisotropic materials for masonry have seen significant progress. Yue *et al*. (2012) modified the yield function of the concrete plastic damage model using the typical yield function model for the masonry material. The modified model is used for nonlinear calculation of the pushover test of an external brick-reinforced concrete frame. The applicability of the modified yield surface plastic damage model in the simulation of energy consumption and damage mode of a masonry structure is also verified using this model. Yang *et al*. (2013) introduced the corresponding model for the damage unit according to the masonry damage mechanism. Based on the results of the whole stress-strain curve test, the stochastic modeling principle and optimization algorithm are determined to evaluate the random field and material parameters. The results of the stress strain relationship and analytical tests are compared to verify the validity of the damage unit model. However, it is not clear whether the model is applied to the study of masonry tension or shear research. Fu and Qian (2018) applied the stress tensor method of linear transformation to develop a constitutive model for masonry materials. On the basis of two damage variables for tension and compression, a new variable is introduced that describes the slip failure of mortar seam TYPE II. This provides accurate real-time information about the distribution state of damage structure and weak parts of the structure. Thus, the validity of the constitutive model in the repair of structural design and usability was verified.

Berto *et al*. (2002) proposed an orthotropic damage model for brittle masonry under plane load, and further defined four independent internal damage parameters, namely, axial tension, axial compression, stiffness recovery at fracture closure, and inelastic behavior at different coordinate axes. The damage field of the material is defined by four equivalent stress values. The regression path from the effective stress to the damage stress is given by the product of the damage parameter and fourth-order damage effect tensor of the effective stress state. Pelà *et al*. (2011) used two stress transformation tensors related to the tensile stress and compressive stress states to establish the orthogonal anisotropic behavior and corresponding relation with the auxiliary model. Two scalar variables are used to monitor local damage under tension and compression in a plane stress mapping space. The model may simulate the anisotropic damage and consider unilateral effect, and thus provides a theoretical basis for building a continuous damage model of orthotropic materials under plane stress conditions. Most of the elastoplastic damage constitutive models proposed in the previous studies are complicated in numerical processing, low in computational efficiency, and poor in stability, which hinder their application in engineering practice.

Compared with the masonry structural constitutive model theory, the constitutive model theory of a concrete structure is relatively mature. There are many studies on the strength failure criterion of concrete, elasto-plastic constitutive theory, and mechanics of fracture damage yielded convincing results. To study the shear performance and failure mode of brick masonry walls under low cyclic reciprocating loads, this study modified and enriched the elastic-plastic damage formula proposed by Faria and Oliver *et al*. (Cervera *et al*.,1996; Faria *et al*., 1998, 2000, 2004), and developed an elastic-plastic damage constitutive model that can take into account the anisotropy characteristics of brick masonry materials. Considering the different properties of masonry in tensile and compressive conditions, the yield functions of tensile and compressive conditions are defined using Rankine strength theory and DP strength theory, respectively. Two different scalar damage variables are introduced into the stress-strain relationship to describe the damage process of tensile and compressive strain states. In this study, the plastic strain evolution equation is established in the effective stress space and the empirical expression is used to calculate the plastic strain. In addition, the Heaviside function was used to consider the unilateral effect of masonry materials under cyclic loading, and the stress update algorithm process was necessarily modified to enable the constitutive model to consider the tensile plastic permanent deformation of masonry materials, which is presented in Section 2.

In Section 3, to verify the correctness of the proposed constitutive model, the numerical simulation of the brick masonry under monotonic and cyclic uniaxial tension and compression loads is described. Section 4 presents a series of numerical simulations that were carried out on four masonry wall specimens with different mortar strength under the action of low cyclic reciprocating loads to verify the applicability of the model in response to the structure of the wall specimens. Finally, concluding remarks are given in Section 5.

2 Basic theory of elastoplastic damage model

2.1 Fundamentals of continuous damage mechanics

During the manufacturing process of engineering materials, various micro-defects (micro-cracks and micro-voids) occur inside the materials. The use of these engineering structures causes the micro-defects to further expand or develop, resulting in the gradual deterioration of mechanical properties of the materials (Shang *et al*., 2020; Liu *et al*., 2020; Gong *et al*., 2021; Li and Tong, 2021). The internal defects of the material are called "damages". The expansion of internal defects under the action of external forces is called damage evolution, which is an irreversible and energy-consuming process. The brick masonry material produces irreversible deformation and exhibits ductile behavior under lateral pressure. The plasticity theory clearly reflects these properties, but the plasticity model does not indicate the decline in stiffness of the masonry materials. The damage theory describes the development of internal defects in materials, where the model based on the theory reflects

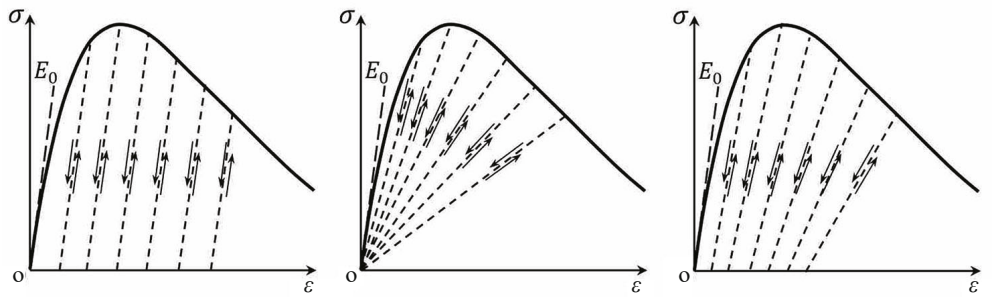

(a) Elastoplastic material (b) Elastic damage material (c) Elastoplastic damage material

Fig. 1 Strength and stiffness anistropy

the decrease in stiffness. However, it cannot replace the plasticity theory to explain the irreversible deformation of materials. Based on the combination of plasticity and damage theories, the constitutive model for the elasto-plastic damage of masonry is derived from stiffness degradation and plastic deformation. Figure 1 depicts the anisotropic characteristics of strength and stiffness of various materials.

According to the theory of continuous damage mechanics (as shown in Fig. 2), the damage variable d is used to describe the process of formation, development, and final failure of micro defects.

$$d = \frac{S - \bar{S}}{S} \tag{1}$$

When isotropic damage is considered, it is assumed that the microdefects are uniformly distributed in all directions. Here, σ is the nominal stress (Cauchy stress) on the initial section S. Due to the existence of damage, the actual stress on the undamaged section $\bar{S}$ is

$$\bar{\sigma} = \frac{\sigma}{(1-d)} \tag{2}$$

where the damage variable $d \in [0, 1]$, 0 represents that the material is intact and 1 represents the total damage of the material, and $\bar{\sigma}$ refers to the effective stress.

It is assumed that the material in the undamaged area obeys the general stress-strain relationship. Even though the damage in the material is only related to the elastic deformation, it also affects the plastic deformation of the material. The total strain tensor is the sum of the elastic strain tensor and plastic strain tensor in the nonlinear development of the material under stress

$$\boldsymbol{\varepsilon} = \boldsymbol{\varepsilon}^{\mathrm{e}} + \boldsymbol{\varepsilon}^{\mathrm{p}} \tag{3}$$

where $\boldsymbol{\varepsilon}$ is the total strain tensor; $\boldsymbol{\varepsilon}^{\mathrm{e}}$ is the corresponding elastic strain tensor; and $\boldsymbol{\varepsilon}^{\mathrm{p}}$ is the corresponding plastic strain tensor.

According to the strain equivalence principle of effective stress, $\bar{\boldsymbol{\sigma}}$ is expressed as

$$\bar{\boldsymbol{\sigma}}\left(\boldsymbol{\varepsilon}, \boldsymbol{\varepsilon}^{\mathrm{p}}\right) = \boldsymbol{D}_0 : \left(\boldsymbol{\varepsilon} - \boldsymbol{\varepsilon}^{\mathrm{p}}\right) \tag{4}$$

where $\boldsymbol{D}_0$ is the elastic constitutive matrix of the undamaged material. Thus, the Cauchy stress is expressed as

$$\boldsymbol{\sigma} = 1 - d\bar{\boldsymbol{\sigma}} = 1 - d\boldsymbol{D}_0 : \left(\boldsymbol{\varepsilon} - \boldsymbol{\varepsilon}^{\mathrm{p}}\right) \tag{5}$$

The above equation is the stress-strain relationship with damage variables termed as the damage constitutive relationship.

2.2 Effective stress split and Helmholtz free energy potential

The masonry materials exhibit strength anisotropy and stiffness (unilateral effect) under the action of tensile and compressive stress, which is similar to the characteristics of concrete. Therefore, this study adopts the spectral split method of Faria and Oliver for effective stress to reflect these characteristics. It is assumed that the tensile stress causes tensile damage, and compressive stress causes compression damage. In complex loading, the damage is a combination of tensile and compression damage.

$$\bar{\boldsymbol{\sigma}}^{+} = \sum_i \langle \bar{\sigma}_i \rangle \boldsymbol{P}_i \boldsymbol{P}_i^{\mathrm{T}} \tag{6}$$

$$\bar{\boldsymbol{\sigma}}^{-} = \bar{\boldsymbol{\sigma}} - \bar{\boldsymbol{\sigma}}^{+} \tag{7}$$

where $\bar{\boldsymbol{\sigma}}^{+}$ and $\bar{\boldsymbol{\sigma}}^{-}$ represent the tension and compression components of effective stress, respectively, $\langle . \rangle$ is the Macaulay parentheses for the calculation of $\langle x \rangle = (x + |x|)/2$, and $\boldsymbol{P}_i$ is the unit column vector in the principal direction of the effective force.

Material damage is an irreversible thermodynamic process, which is a purely mechanical isothermal process upon the exclusion of heat dissipation. The Helmholtz free energy potential ψ of the material for strain tensor $\boldsymbol{\varepsilon}$, and damage variable d state function (Lemaitre, 2000) is expressed as:

$$\psi = \psi(\boldsymbol{\varepsilon}, d) = (1-d)\psi_0(\boldsymbol{\varepsilon}) \tag{8}$$

where $\psi_0(\boldsymbol{\varepsilon})$ is the initial Helmholtz free energy potential of the damaged material, which is also the equal strain energy W, given by

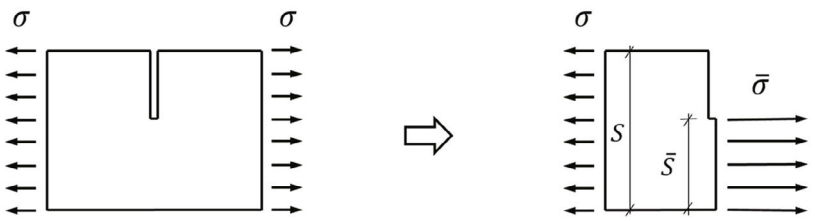

Fig. 2 Principle of effective stress and strain equivalence

$$\psi_0(\boldsymbol{\varepsilon}) = W(\boldsymbol{\varepsilon}) = \frac{1}{2}\boldsymbol{\varepsilon}:\ \boldsymbol{E}_0:\ \boldsymbol{\varepsilon} = \frac{1}{2}\bar{\boldsymbol{\sigma}}:\ \boldsymbol{C}_0:\ \bar{\boldsymbol{\sigma}} \tag{9}$$

Based on the positive and negative components of effective stress tensor, the initial Helmholtz free energy potential of the material is split into ψ_0^+, and ψ_0^-, which is expressed as the sum in the following equation.

$$\psi_0\boldsymbol{\varepsilon} = \psi_0^+(\boldsymbol{\varepsilon}) + \psi_0^-(\boldsymbol{\varepsilon}) \geq 0 \tag{10}$$

In order to describe the damage evolution, which is an irreversible thermodynamics process of energy dissipation, the tensile damage variable d^+ and compression damage variable d^- are introduced to describe materials Helmholtz free energy potential degradation under the effect of force $\bar{\boldsymbol{\sigma}}^+$ and $\bar{\boldsymbol{\sigma}}^-$.

As the initial Helmholtz free energy potential ψ_0^+ and ψ_0^- are nonnegative values, the damage variable can be described as below:

$$0 \leq (d^+,\ d^-) \leq 1 \tag{11}$$

Then, the total Helmholtz free energy potential of the material can be expressed as:

$$\begin{aligned}&\psi(\boldsymbol{\varepsilon},\ d^+, d^-) = \psi^+(\boldsymbol{\varepsilon},\ d^+) + \psi^-(\boldsymbol{\varepsilon},\ d^-) = \\ &(1-d^+)\psi_0^+(\boldsymbol{\varepsilon}) + (1-d^-)\psi_0^-(\boldsymbol{\varepsilon}) \geq 0\end{aligned} \tag{12}$$

2.3 Damage variables and their evolution criteria

By the introduction of the tensile damage variable d^+ and compression damage variable d^-, the evolution law of the two damage variables is given to form a complete elastic-plastic damage stress-strain relationship. In this study, the damage evolution criteria were established based on the energy release rate of the damage (Li and Wu, 2005; Wu *et al*., 2006). The damage energy release rate controls the damage evolution alone. The nature of the damage is not affected by the equivalent transformation. This study adopted the equivalent expression given by Faria and Oliver *et al*. (1998).

The damage energy release rates under tension (Y^+) and compression (Y^-) are defined as follows:

$$Y^+ = -\frac{\partial\psi}{\partial d^+} = -\frac{\partial\psi^+}{\partial d^+} = \sqrt{(\bar{\boldsymbol{\sigma}}^+)^{\mathrm{T}}\boldsymbol{D}_0^{-1}(\bar{\boldsymbol{\sigma}}^+)} \tag{13a}$$

$$Y^- = -\frac{\partial\psi}{\partial d^-} = -\frac{\partial\psi^-}{\partial d^-} = \sqrt{3}\left(K\bar{\sigma}_{\mathrm{oct}} + \bar{\tau}_{\mathrm{oct}}\right) \tag{13b}$$

where $\bar{\sigma}_{\mathrm{oct}}$ is the octahedral normal stress, $\bar{\tau}_{\mathrm{oct}}$ is the octahedral shear stress, and K is the material constant.

$$K = \sqrt{2} \times \frac{1-R_0}{1-2R_0} \tag{14}$$

where R_0 is the ratio of the concrete biaxial isobaric strength to the uniaxial compressive strength.

Based on the definition of equivalent stress and the technique inspired by Simo and Ju (1987, 1989), two independent damage potential functions, G^+ and G^- are introduced to determine the damage state of the material. G^+ is used for stretching, and G^- for compression:

$$G^+(Y^+,\ r_n^+) = g^+(Y^+) - g^+(r_n^+) \leq 0 \tag{15a}$$

$$G^-(Y^-,\ r_n^-) = g^-(Y^-) - g^-(r_n^-) \leq 0 \tag{15b}$$

$G^+(Y^+, r_n^+) = 0$ and $G^-(Y^-, r_n^-) = 0$ is used to determine the damaged surface, $Y^\pm$ at a certain moment of n represents the damage energy release rates of the material, the variables r_n^+ and r_n^- represent the maximum damage energy release rate obtained before time n, and is termed as the historical maximum damage energy release rate or current damage energy release rate threshold. These parameters control the size of the expanded damage surface and are expressed as

$$r_n^\pm = max\left\{r_0^\pm,\ \max_{\theta\in[0,\ n]} Y_\theta^\pm\right\} \leq 0 \tag{16}$$

The material enters a nonlinear state as the damage energy release rate $Y^\pm$ exceeds the threshold of the initial damage energy release rate $r_0^\pm$. Further damage is observed in the material as the damage energy release rate $Y^\pm$ exceeds the historical maximum damage energy release rate $r_n^\pm$. The initial damage thresholds of tension and compression are the characteristic properties of the material. For any time n, $r_n^\pm \geq r_0^\pm$. The initial damage thresholds of tension and compression are defined as

$$r_0^{\ +} = \frac{f_{\mathrm{t}}}{\sqrt{E}} \tag{17}$$

$$r_0^{\ -} = \sqrt{\sqrt{\frac{2}{3}}\frac{R_0}{1-2R_0}f_0} \tag{18}$$

where f_{t} and f_0 are the initial yield strength under tension and pressure, respectively, and E is the elastic modulus of masonry.

The evolution of the damage variables is obtained by the introduction of orthogonal flow criteria, which are expressed as follows.

$$\dot{d}^{\pm} = \dot{\lambda}^{d\pm} \frac{\partial g^{\pm}}{\partial Y^{\pm}} \tag{19}$$

$$\dot{r}_n^{\pm} = \dot{\lambda}^{d\pm} \tag{20}$$

where the damage evolution factor $\dot{\lambda}^{d\pm}$ is a non-negative scalar subjected to the loading and unloading rule, and expressed according to the Kuhn-Tucker condition:

$$\dot{\lambda}^{d\pm} \geq 0 \qquad G^{\pm} \leq 0 \qquad \dot{\lambda}^{d\pm} G^{\pm} = 0$$

The material is in the stage of damage unloading or neutral variable loading for $G^{\pm} < 0$, $\dot{\lambda}^{d\pm} = 0$, and $\dot{d}^{\pm} = 0$ with no further development of damage. When the fracture is under load, $G^{\pm} = 0$, and $\dot{\lambda}^{d\pm} > 0$, which are obtained by the damage consistency condition $\dot{G}^{\pm} = 0$.

Based on the characteristics of the damage variables $d^{\pm}$, the potential function $g^{\pm}\left(r^{\pm}\right)$ must meet the following requirements:

$$0 \leq g^{\pm}\left(r^{\pm}\right) \leq 1 \qquad g^{\pm}\left(r_0^{+}\right) = 0 \qquad \dot{g}^{\pm}\left(r^{\pm}\right) \geq 0$$

According to the uniaxial tension and compression tests, the basic forms of $d^{\pm}$ were established. The empirical relationship proposed by Oliver *et al*. (1990) and Faria *et al*. (1998) was used to reflect the changing relationship between the damage variables $d^{\pm}$ and damage energy release rates $r_n^{\pm}$:

$$d^{+} = 1 - \frac{r_0^{+}}{r_n^{+}} \exp\left[A^{+}\left(1 - \frac{r_n^{+}}{r_0^{+}}\right)\right], \; r_n^{+} \geq r_0^{+} \tag{21}$$

$$d^{-} = 1 - \frac{r_0^{-}}{r_n^{-}}\left(1 - A^{-}\right) - A^{-} \exp\left[B^{-}\left(1 - \frac{r_n^{-}}{r_0^{-}}\right)\right], \; r_n^{-} \geq r_0^{-} \tag{22}$$

where A^{+} is the model parameter for the evolution equation of tensile damage, and A^{-} and B^{-} are the model parameters for the compression damage evolution equation, respectively.

The fracture energy concept is introduced to the parameter to avoid the grid sensitivity of the calculated results, which is defined as

$$A^{+} = \left(\frac{G_{\mathrm{f}} E}{l_{\mathrm{c}} f_{\mathrm{t}}^{2}} - 0.5 \right)^{-1} \geq 0 \tag{23}$$

where G_{f} is the tensile fracture energy of masonry, l_{c} is the characteristic length of cracks associated with meshing, and $l_{\mathrm{c}} = \sqrt[3]{V}$, and V is the entity unit volume in the $\sqrt[3]{V}$ term.

Thus, the combined formula for tensile and compressive damages proposed by Faria and Oliver *et al*. is

$$\boldsymbol{\sigma} = 1 - d^{+}\bar{\boldsymbol{\sigma}}^{+} + 1 - d^{-}\bar{\boldsymbol{\sigma}}^{-} \tag{24}$$

2.4 Material yield conditions and loading-unloading criteria

In view of the different yield characteristics, different yield surface forms were adopted herein to consider the tensile and compressive characteristics of masonry materials.

The maximum tensile stress theory proposed by Rankine in 1858 was adopted as the tensile criterion for the material model. The criterion failed as the maximum tensile stress approached the tensile strength in either principal stress directions, which is expressed as follows:

$$F^{+}\left(\bar{\boldsymbol{\sigma}}_{ij}\right) = \sigma_1 - f_{\mathrm{t}} = 0 \tag{25}$$

where σ_1 is the maximum tensile stress in the direction of the principal stress, and f_{t} is the tensile strength of the material.

The compression criterion for the material model was developed using the Drucker-Prager theory (1952), the Von Mises theory of circular partial plane envelope, and the Mohr-Coulomb theory of linear meridian combination for the formation of the failure envelope. The yield surface form in the equivalent stress space is:

$$F^{-}\left(\bar{\boldsymbol{\sigma}}_{ij}\right) = f\left(\bar{I}_1, \bar{J}_2\right) = \alpha \bar{I}_1 + \sqrt{\bar{J}_2} - k = 0 \tag{26}$$

where α and k are material constants, $\bar{I}_1$ is the first invariant stress tensor, and $\bar{J}_2$ is the partial invariant

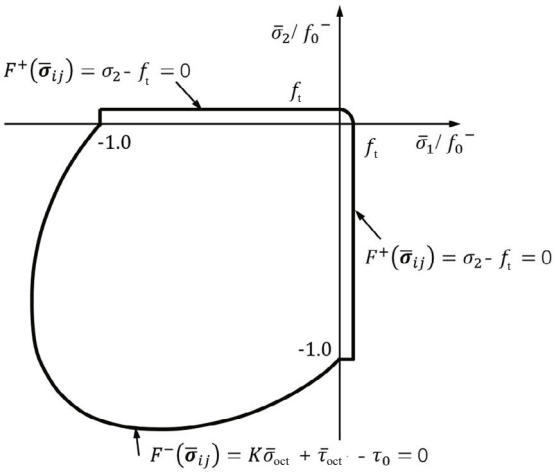

Fig. 3 Yield surface in plane stress space

stress tensor with octahedral normal stress and shear stress ($\bar{\sigma}_{\text{oct}}$ and $\bar{\tau}_{\text{oct}}$) for linear substitution. This is further expressed as:

$$F^{-}\left(\bar{\boldsymbol{\sigma}}_{ij}\right)=K\bar{\sigma}_{\text{oct}}+\bar{\tau}_{\text{oct}}-\tau_0=0 \tag{27}$$

where $\tau_0=\dfrac{\sqrt{2}}{3}\dfrac{R_0}{1-2R_0}f_0$, and K and f_0 are the constant for compression of the material, and initial yield strength, respectively.

The shape of the above yield surface function in plane stress space is shown in Fig. 3.

As shown in Fig. 4, the material is in an elastic state for the condition of $F\left(\bar{\boldsymbol{\sigma}}_{ij}\right)<0$. When $F\left(\bar{\boldsymbol{\sigma}}_{ij}\right)=0$, the corresponding loading, neutral variable load, and unloading are expressed as:

Loading: $\dfrac{\partial F}{\partial\sigma_{ij}}\mathrm{d}\sigma_{ij}>0,\ \mathrm{d}\varepsilon_{ij}^{\mathrm{P}}\neq 0$

Neutral variable load: $\dfrac{\partial F}{\partial\sigma_{ij}}\mathrm{d}\sigma_{ij}=0,\ \mathrm{d}\varepsilon_{ij}^{\mathrm{P}}=0$

Unloading: $\dfrac{\partial F}{\partial\sigma_{ij}}\mathrm{d}\sigma_{ij}<0,\ \mathrm{d}\varepsilon_{ij}^{\mathrm{P}}=0$

2.5 Solution of plastic strain

In this study, the plastic strain evolution equation was established under the effective stress space. The complexity in processing the softening segment is avoided by directly applying the plastic mechanical method for nonlinear analysis due to its calculation efficiency (Lee and Fenves, 2001). The empirical expression was used to calculate the plastic strain (Faria *et al*., 1998, 2004; Valliappan *et al*., 1999; Hatzigeorgio *et al*., 2001).

$$\dot{\boldsymbol{\varepsilon}}^{\mathrm{P}}=\beta EH\left(\dot{d}^{\pm}\right)\frac{\left\langle\bar{\boldsymbol{\sigma}}:\dot{\boldsymbol{\varepsilon}}\right\rangle}{\bar{\boldsymbol{\sigma}}:\bar{\boldsymbol{\sigma}}}\boldsymbol{D}_0^{-1}:\bar{\boldsymbol{\sigma}} \tag{28}$$

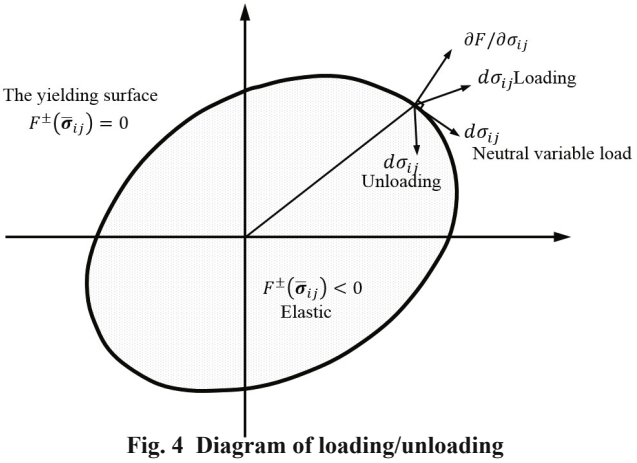

Fig. 4 Diagram of loading/unloading

For $\mathbf{1}_{\bar{\boldsymbol{\sigma}}}=\dfrac{\bar{\boldsymbol{\sigma}}}{\sqrt{\bar{\boldsymbol{\sigma}}:\bar{\boldsymbol{\sigma}}}}$, the expression is given by:

$$\dot{\boldsymbol{\varepsilon}}^{\mathrm{P}}=\beta EH\left(\dot{d}^{\pm}\right)\left\langle\mathbf{1}_{\bar{\boldsymbol{\sigma}}}:\dot{\boldsymbol{\varepsilon}}\right\rangle\boldsymbol{D}_0^{-1}:\mathbf{1}_{\bar{\boldsymbol{\sigma}}} \tag{29}$$

where β is the material parameter that controls the plastic strain with values, $\beta\geq 0$, E is the elastic modulus of the material, $H(.)$ is the Heaviside function, $\langle.\rangle$ represent the Macaulay parentheses, $\bar{\boldsymbol{\sigma}}:\dot{\boldsymbol{\varepsilon}}$ is always a non-negative dissipative value, and $\boldsymbol{D}_0^{-1}$ is the effective flexibility tensor. The formula simplifies the calculation of plastic strain. It has the following characteristic features:

1) The establishment method of the plastic model in this study greatly improves the calculation efficiency and numerical stability of the model.

2) Equation (29) is different from the original plastic strain expression, which simultaneously considers the plastic tensile and compressive strain. The compression and tension damage develops under conditions of $\dot{d}^{\pm}>0$, $H\left(\dot{d}^{\pm}\right)>0$. When $\dot{\boldsymbol{\varepsilon}}^{\mathrm{P}}>0$, the plastic strain develops, otherwise $\dot{\boldsymbol{\varepsilon}}^{\mathrm{P}}=0$.

The numerical algorithm of the elastic-plastic constitutive model is performed to determine the elastic trial stress given by Eq. (30).

$$\bar{\boldsymbol{\sigma}}_{n+1}^{\text{trial}}=\bar{\boldsymbol{\sigma}}_n+\boldsymbol{D}_0:\Delta\boldsymbol{\varepsilon} \tag{30}$$

Substituting the derivative of Eq. (4) into Eq. (29) results in the expression for effective stress increment given by:

$$\begin{aligned}\dot{\bar{\boldsymbol{\sigma}}}&=\boldsymbol{D}_0\left(\dot{\boldsymbol{\varepsilon}}-\dot{\boldsymbol{\varepsilon}}^{\mathrm{P}}\right)\\&=\boldsymbol{D}_0\left(\dot{\boldsymbol{\varepsilon}}-\beta EH\left(\dot{d}^{\pm}\right)\left\langle\mathbf{1}_{\bar{\boldsymbol{\sigma}}}:\dot{\boldsymbol{\varepsilon}}\right\rangle\boldsymbol{D}_0^{-1}:\mathbf{1}_{\bar{\boldsymbol{\sigma}}}\right)\\&=\boldsymbol{D}_0:\dot{\boldsymbol{\varepsilon}}-\beta EH\left(\dot{d}^{\pm}\right)\left\langle\mathbf{1}_{\bar{\boldsymbol{\sigma}}}:\dot{\boldsymbol{\varepsilon}}\right\rangle\mathbf{1}_{\bar{\boldsymbol{\sigma}}}\end{aligned} \tag{31}$$

The effective stress tensor at t_{n+1}

$$\begin{aligned}\bar{\boldsymbol{\sigma}}_{n+1}&=\bar{\boldsymbol{\sigma}}_n+\boldsymbol{D}_0:\Delta\boldsymbol{\varepsilon}-\\&\beta EH\left(\dot{d}_{n+1}^{\pm}\right)\left\langle\bar{\boldsymbol{\sigma}}_{n+1}:\Delta\boldsymbol{\varepsilon}\right\rangle\frac{\bar{\boldsymbol{\sigma}}_{n+1}}{\bar{\boldsymbol{\sigma}}_{n+1}:\bar{\boldsymbol{\sigma}}_{n+1}}\end{aligned} \tag{32}$$

An equivalent linear transformation is performed on Eq. (32)

$$\bar{\boldsymbol{\sigma}}_{n+1}=\lambda\bar{\boldsymbol{\sigma}}_{n+1}^{\text{trial}} \tag{33}$$

where λ is the plastic flow factor.

Therefore, the effective stress completes an incremental step update.

$$\lambda = 1 - \frac{\beta}{\left\|\bar{\boldsymbol{\sigma}}_{n+1}^{\text{trial}}\right\|} EH\left(\dot{d}_{n+1}^{\pm}\right)\left\langle \mathbf{1}_{\bar{\boldsymbol{\sigma}}_{n+1}^{\text{trial}}} : \Delta\boldsymbol{\varepsilon} \right\rangle \tag{34}$$

2.6 Stress update algorithm of the damage model

To summarize the above theory, the flow chart of stress updating algorithm for the elastoplastic damage constitutive relationship of masonry materials (see Fig. 5) is as follows:

Step $n=0$:

(i) Set the initial conditions $r_n^+ = r_0^+$, $r_n^- = r_0^-$, $d_n^+ = 0$, $d_n^- = 0$.

Step $n+1$:

(ii) According to Eq. (30), compute the elastic trial stress $\bar{\boldsymbol{\sigma}}_{n+1}^{\text{trial}} = \bar{\boldsymbol{\sigma}}_n + \boldsymbol{D}_0 : \Delta\boldsymbol{\varepsilon}$.

(iii) According to Eqs. (6) and (7), split $\bar{\boldsymbol{\sigma}}_{n+1}^{\text{trial}}$ into $\left(\bar{\boldsymbol{\sigma}}_{n+1}^{\text{trial}}\right)^+$ and $\left(\bar{\boldsymbol{\sigma}}_{n+1}^{\text{trial}}\right)^-$, evaluate $F^{\pm}\left(\bar{\boldsymbol{\sigma}}_{ij}\right)$ using Eqs. (25) and (27). Is $F^+\left(\bar{\boldsymbol{\sigma}}_{ij}\right) > 0$ (or $F^-\left(\bar{\boldsymbol{\sigma}}_{ij}\right) > 0$)?

If neither condition is satisfied, the plasticity is not entered, do not evaluate d^+, d^-, and $\boldsymbol{\varepsilon}^{\text{P}}$. $\bar{\boldsymbol{\sigma}}_{n+1} = \bar{\boldsymbol{\sigma}}_{n+1}^{\text{trial}}$, go to the damage correction step (vi).

Otherwise, step (iv) is executed.

(iv) Compute $\left\|\bar{\boldsymbol{\sigma}}_{n+1}^{\text{trial}}\right\|$ and $\mathbf{1}_{\bar{\boldsymbol{\sigma}}_{n+1}^{\text{trial}}} = \bar{\boldsymbol{\sigma}}_{n+1}^{\text{trial}} / \left\|\bar{\boldsymbol{\sigma}}_{n+1}^{\text{trial}}\right\|$. Is $\left\langle \mathbf{1}_{\bar{\boldsymbol{\sigma}}_{n+1}^{\text{trial}}} : \Delta\boldsymbol{\varepsilon} \right\rangle > 0$?

Yes: Plastic evolution may occur, admitting $H\left(\dot{d}_{n+1}^{\pm}\right) = 1$. Compute λ and $\hat{\boldsymbol{\sigma}} = \lambda\bar{\boldsymbol{\sigma}}_{n+1}^{\text{trial}}$ with Eqs. (34) and (33), step (v) is executed.

No: No plastic evolution occurred. $\bar{\boldsymbol{\sigma}}_{n+1} = \bar{\boldsymbol{\sigma}}_{n+1}^{\text{trial}}$, go to the damage correction step (vi).

(v) Split $\hat{\boldsymbol{\sigma}}$ into $\hat{\boldsymbol{\sigma}}^+$ and $\hat{\boldsymbol{\sigma}}^-$. Compute the damage energy release rates $Y^-\left(\hat{\boldsymbol{\sigma}}^-\right)$ and $Y^+\left(\hat{\boldsymbol{\sigma}}^+\right)$ with Eq. (13). Is $Y^-\left(\hat{\boldsymbol{\sigma}}^-\right) > r_n^-$ (or $Y^+\left(\hat{\boldsymbol{\sigma}}^+\right) > r_n^+$)?

Yes: Once either condition is satisfied, damage evolution occurred, $\bar{\boldsymbol{\sigma}}_{n+1} = \hat{\boldsymbol{\sigma}}$, go to the damage correction step (vi).

No: No damage evolution occurred, $\bar{\boldsymbol{\sigma}}_{n+1} = \bar{\boldsymbol{\sigma}}_{n+1}^{\text{trial}}$, go to the damage correction step (vi).

(vi) Split $\bar{\boldsymbol{\sigma}}_{n+1}$, into $\bar{\boldsymbol{\sigma}}_{n+1}^+$ and $\bar{\boldsymbol{\sigma}}_{n+1}^-$.

(vii) Compute Y_{n+1}^+ and Y_{n+1}^- according to Eq. (13).

(viii) If $Y_{n+1}^+ > r_n^+$ or $Y_{n+1}^- > r_n^-$, update damage thresholds: $r_{n+1}^+ = max\left\{r_n^+,\ Y_{n+1}^+\right\}$ or $r_{n+1}^- = max\left\{r_n^-,\ Y_{n+1}^-\right\}$, update damage variables $d_{n+1}^+ = G\left(r_{n+1}^+\right)$ and $d_{n+1}^- = G\left(r_{n+1}^-\right)$ according to Eqs. (21) and (22).

Otherwise, step (ix) is executed.

(ix) Finally, compute the Cauchy stress tensor

$$\boldsymbol{\sigma}_{n+1} = \left(1 - d_{n+1}^+\right)\bar{\boldsymbol{\sigma}}_{n+1}^+ + \left(1 - d_{n+1}^-\right)\bar{\boldsymbol{\sigma}}_{n+1}^- \cdot \text{EXIT}$$

Under the LS-DYNA platform, a subroutine for the elasto-plastic damage model of masonry materials is programmed according to the above stress update algorithm. Numerical verification and structural response analysis under the pseudo-static load of masonry walls are carried out using the programmed subroutine.

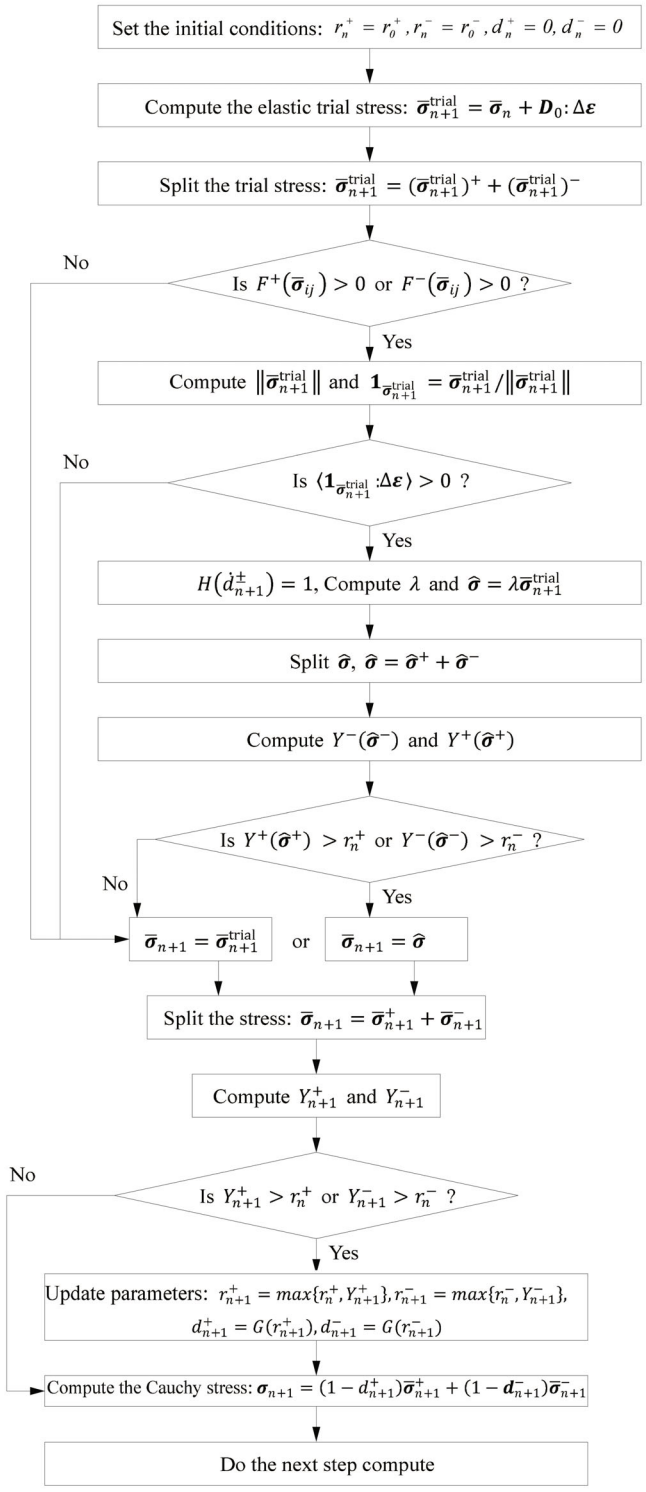

Fig. 5 Basic flow of numerical calculation of elastic-plastic damage constitutive model

3 Preliminary verification of the model under simple stress

3.1 Uniaxial compression and tension monotonic loading

To verify the correctness of the constitutive model, a uniaxial tensile and compressive model of masonry materials was established using the masonry test data (Yi and Li, 2006) for numerical verification. Solid element is adopted to build the model. The size of the specimen is 365 mm length × 240 mm width × 746 mm height. The elastic modulus of the material is 2704 MPa. The Poisson′s ratio is 0.2. The uniaxial compressive yield strength f_c is 1.30 MPa and the uniaxial tensile yield strength f_t is 0.224 MPa.

To further verify the validity of the constitutive model, the curves obtained by numerical simulation herein were compared with the experimental results and theoretical formula curves proposed by Zheng *et al*. (2011) and Yang *et al*. (2013). The theoretical formula curve in Fig. 6, which is the masonry tensile constitutive curve proposed by Zheng, is based on the tensile stress-strain curve of concrete and has been improved. The theoretical formula takes the rising section as a linear line. The falling section takes that of the concrete tension curve after parameter correction. It can be seen from Fig. 3 that the tensile stress-strain curve acquired from the model proposed in this study is in good agreement with the theoretical curve, except for the shape of the falling section curve.

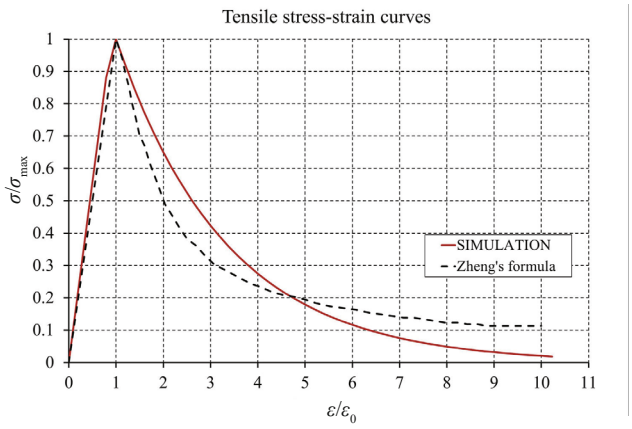

Fig. 6 Uniaxial tensile stress-strain curve

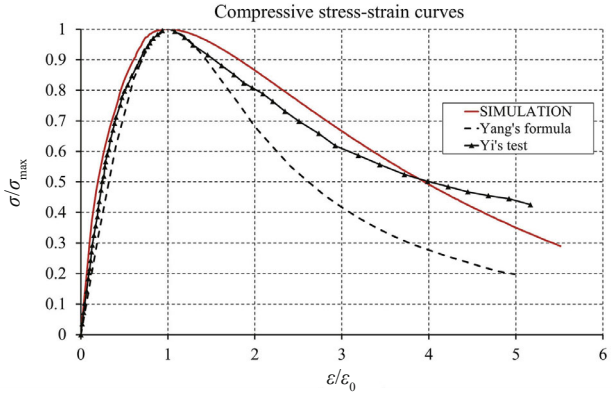

Fig. 7 Uniaxial compression stress-strain curve

Figure 7 shows the compressive stress-strain curve comparison. The theoretical formula curve in this figure is the stochastic stress-strain relationship of compression put forward by Yang based on the stochastic modeling principle and optimization algorithm to determine random field parameters and material parameters. Compared with the test curve (Yi and Li, 2006), the theoretical curve is in good agreement at the rising section, but decreases much faster than the test results at the falling section. Meanwhile, the curve acquired from the model proposed herein shows better agreement with the test results at the falling section.

3.2 Uniaxial compression and tension cyclic loading

The whole-process curve of the numerical model determined by the method in this study under cyclic

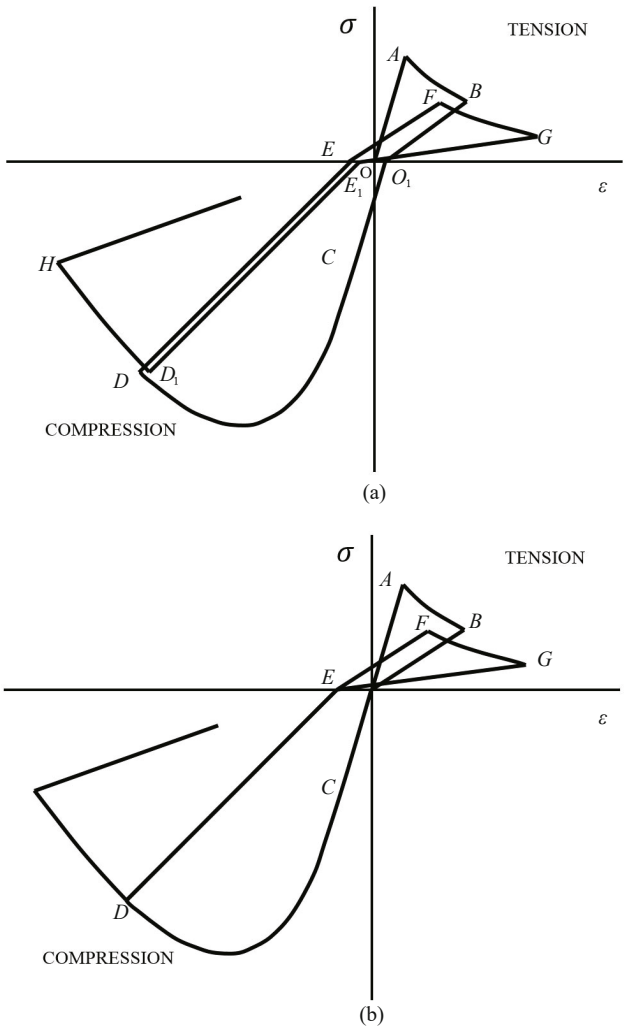

Fig. 8 (a) Numerical model is repeatedly loaded; (b) Faria model is repeatedly loaded

tensile and compressive loads is shown in Fig. 8(a). Meanwhile, the corresponding curve of the Faria model is given in Fig. 8(b). Compared with the Faria model (1998), the model proposed herein can simultaneously consider plastic permanent deformation in both compressive and tensile stages.

The loading sequence for the model is as follows: one loading and unloading under tension ($OABO_1$), one loading and unloading processes under compression (O_1CDE), two loading and unloading processes under tension ($EFGE_1$), and two loading and unloading processes under compression (E_1D_1H). The structural reaction in the loading process is described as follows:

(1) Path $OABO_1$. In section OA, the undamaged material showed linear elastic property, and after reaching the tensile threshold (point B), the material showed softening property (A-B). The comparison between OA and BO_1 clearly shows that the irreversible damage leads to the reduction of material elastic stiffness. In addition, the initial loading point O and unloading point O_1 do not coincide, indicating that the proposed constitutive model can consider the tensile permanent deformation.

(2) Path O_1CDE. When the material is subjected to compressive loading after the tensile damage, the stiffness returns to the initial stiffness ($O_1C//OA$, unilateral effect). Before reaching the compressive damage threshold, the material remains in an elastic state. After reaching the compressive damage threshold, the material shows nonlinear hardening and softening phenomenon.

(3) Path $EFGE_1$. During the secondary tensile loading, the elastic stiffness of the material due to irreversible damage under compression is further reduced. Under the same tensile loading, the loading starting point E and unloading point E_1 do not coincide.

(4) Path E_1D_1H. In the process of secondary compressive loading, due to the closure of the tensile cracks, the compression stiffness and strength are restored ($E_1D_1//ED$), but the damage threshold can only be restored to the level after the damage of the first compression loading.

Comparing Fig. 8(a) with Fig. 8(b), it can be seen that the introduction of tensile damage criterion into the modified model of plastic flow in this study can not only account for the compression permanent deformation but also the tensile permanent deformation, so as to obtain the shear calculation and analysis ability of masonry structure walls.

4 Nonlinear static reaction of masonry walls

4.1 Specimen design

The applicability of the numerical model was verified using some specimens described in the literature (Tang *et al*., 2017) for numerical simulation. All the specimens have the same dimensions of 1645 mm × 1061 mm × 240 mm with an aspect ratio of 0.66, as shown in Fig. 9. The test specimens were set between the base concrete beam and top-loading beam that are cast in-situ with C30 concrete. In the numerical simulation, the top beam was set to facilitate load application in the model. The bottom of the wall was restrained. The bottom beam was assumed to be the fixed boundary, as shown in Fig. 10. In this study, four pieces of wall specimens with different masonry mortar grades under the same pressure effect were selected for numerical simulation. The parameters are shown in Table 1.

Table 1 Specimen parameters

Number	t (mm)	Mortar	Blocks	σ_v (MPa)
EW-0.4-0-0.3	240	M0.4	MU10	0.3
EW-1.0-0-0.3	240	M1.0	MU10	0.3
EW-2.5-0-0.3	240	M2.5	MU10	0.3
EW-5.0-0-0.3	240	M5.0	MU10	0.3

Note: t is wall thickness; σ_v is the vertical pressure at the wall top.

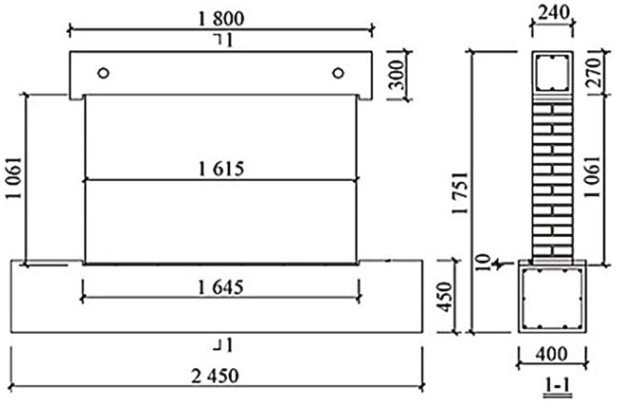

Fig. 9 Geometry dimension of the test specimen

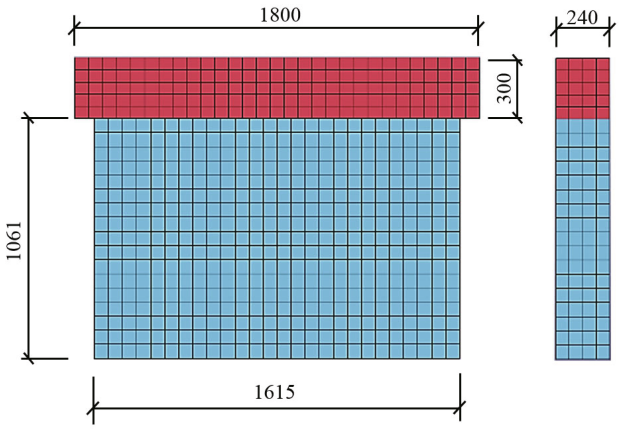

Fig. 10 Specimen in numerical simulation

4.2 Establishment of the numerical model

In this study, a numerical model was established to examine the large deformation behavior of brick masonry walls using the explicit integration algorithm. The universal finite element software LS-DYNA was used to analyze the bearing and deformation capacities of the masonry walls. Solid elements were used to build the numerical model and simulate the brick wall. The wall facade is divided into 26 × 17 meshes, and it is divided into four meshes at the thickness direction. The size of each unit is 62 mm × 62.5 mm × 60 mm. The loading beam and brick wall are connected parallel to each other, The rotation of the loading beam is constrained. The rotation and displacement degrees of the wall bottom have also been constrained. The loading beam is first subjected to a vertical stress of 0.3 MPa and the stress remained constant in the test. A cyclic horizontal displacement load is then applied to the loading beam. The horizontal cyclic load is applied by the displacement control method. To keep consistent with the experiment, the maximum displacement at each stage of the displacement load is set equal to the maximum displacement obtained from the experiment at

Table 2 Constitutive model parameters of brick block materials

	R_d (kg/m^3)	E_0 (GPa)	P_R	R_0	f_{0t} (MPa)	f_{0c} (MPa)	β	G_F (J)	A_c	B_c	A_t
EW-0.4	2000	0.80	0.2	1.0	0.056	–0.910	0.89	240	1.1	0.60	0.01
EW-1.0	2000	1.50	0.2	1.0	0.060	–1.157	0.89	240	1.1	0.60	0.01
EW-2.5	2000	1.95	0.2	1.0	0.090	–1.300	0.89	360	1.1	0.60	0.01
EW-5.0	2000	2.40	0.2	1.0	0.130	–1.500	0.89	360	1.1	0.60	0.01

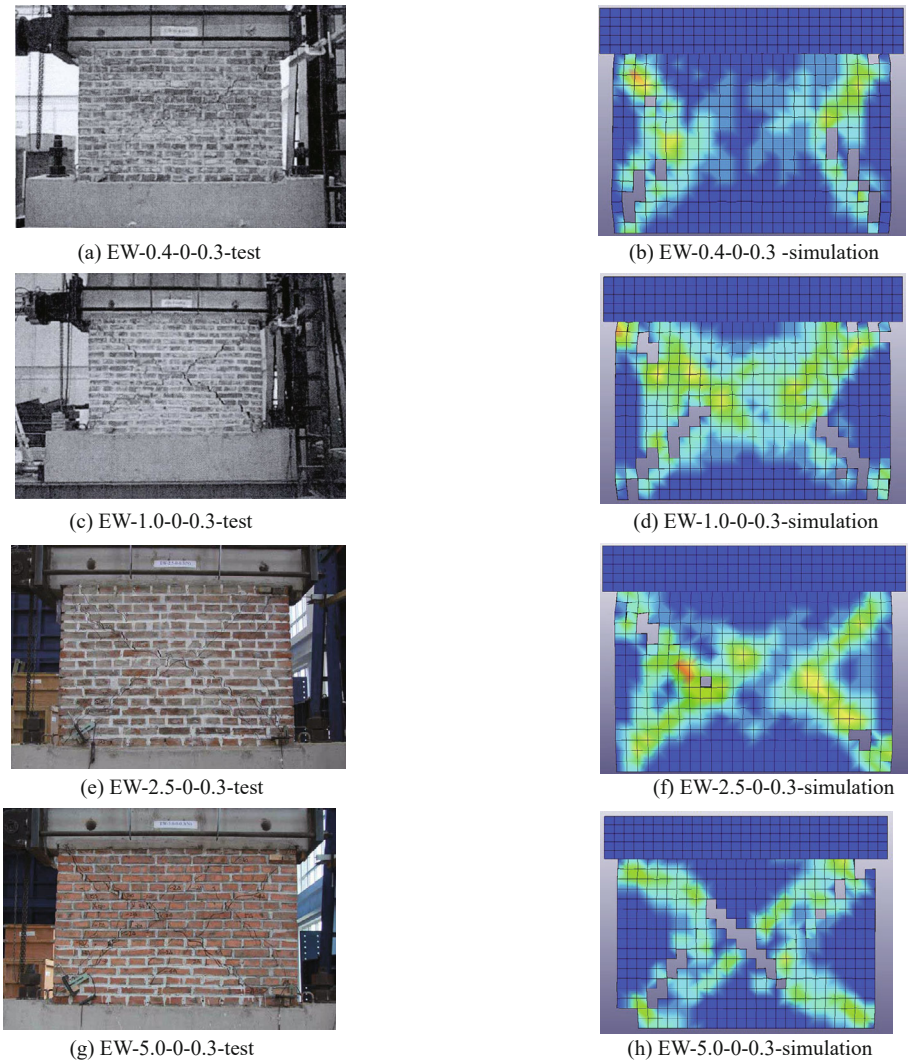

(a) EW-0.4-0-0.3-test (b) EW-0.4-0-0.3 -simulation

(c) EW-1.0-0-0.3-test (d) EW-1.0-0-0.3-simulation

(e) EW-2.5-0-0.3-test (f) EW-2.5-0-0.3-simulation

(g) EW-5.0-0-0.3-test (h) EW-5.0-0-0.3-simulation

Fig. 11 Failure pattern in lab test and numerical simulation

the corresponding load stage.

In the modeling of brick wall materials, the mortar and brick blocks were not distinguished and were assumed as homogeneous materials. A total of 11 parameters of the constitutive model were determined, including the density R_d, elastic modulus E_0, Poisson's ratio P_R, ratio of biaxial compression strength to uniaxial compression strength R_0, tensile yield strength f_{0t}, compressive yield strength f_{0c}, plastic flow constant β, fracture energy G_F, model parameters for compressive damage evolution equation A_c and B_c, and model parameter for tensile damage evolution equation A_t. The element is set to fail when the maximum tensile stress of the element exceeds f_{0t}, or the maximum compressive strain exceeds 0.0023. Table 2 shows the parameters of the four pieces of wall specimens.

4.3 Analysis of the numerical simulation results

The failure morphology and load-displacement hysteretic curve results of masonry wall specimens were compared with the test results, as shown in Figs. 11 and 12. The original wall test and numerical simulation showed shear failure characteristics. The failure patterns are in good agreement with each other.

In Fig. 11, the numerical simulation results are the max-principal tensile strain distribution cloud map and failure element distribution. The analysis results show that all the four walls show shear brittle failure, but the difference is the distribution of shear cracks. For the specimen with mortar strength of 0.4 MPa, under the action of horizontal reciprocating load, the wall forms four max-principal tensile strain distribution bands at the corner, and the angle between the main tensile strain bands and the horizontal line is about 55 degrees. The four max-principal tensile strain distribution bands do not converge in the middle of the wall. When approaching the third positive displacement load (+3 mm), the right lower end corner element reaches the ultimate tensile strain and fails. When approaching the third negative displacement (–3 mm), the left lower end corner element begins to fail, and then more units begin to fail. During the fifth reciprocating displacement loading, the wall also forms a crack zone in the upper corner. After that, the bearing capacity of the wall shows a sharp decline, and then finally fails. The fracture development process and fracture distribution pattern of this specimen are almost the same as the experimental results, as shown in

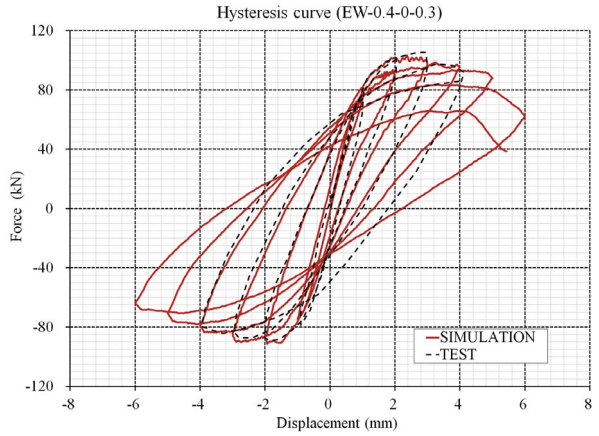

(a) EW -0.4-0-0.3 contrast figure

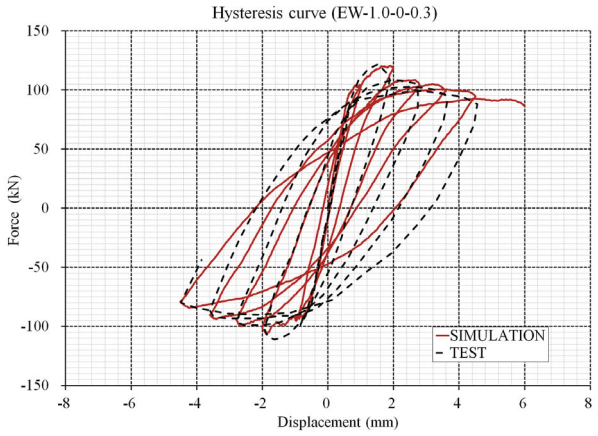

(b) EW-1.0-0-0.3 contrast figure

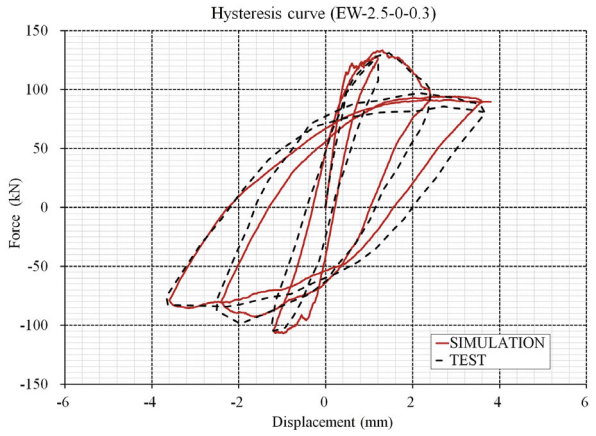

(c) EW-2.5-0-0.3 contrast figure

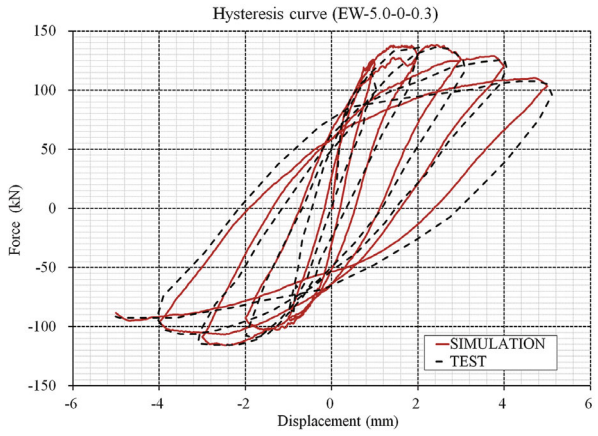

(d) EW-5.0-0-0.3 contrast figure

Fig. 12 Comparison of load-displacement hysteretic curves

Figs.11(a) and 11(b).

For the specimen with mortar strength of 1.0 MPa, the angle between the main tensile strain bands and the horizontal line of the wall is about 45 degrees. The four distribution bands of main tensile strain show an intersection in the middle of the wall, but do not form a diagonal connection. Diagonally through cracks are formed in the test, which are different from the numerical simulation specimens in the shape of crack distribution, as shown in Figs. 11(c) and 11(d). For the specimen with mortar strength 2.5 MPa, when the second positive displacement load reaches 1.6 mm, the corner on the right side of the upper end unit first began to fail, followed by the left side of the upper unit and the right side of the lower unit and the left side of the upper unit and the right side of the lower unit, which are approximately diagonal cracks. The test and numerical results are shown in Figs. 11(e) and 11(f) for contrast.

For the specimen with mortar strength of 5.0 MPa, under the action of reciprocating loads, several main tensile strain distribution bands are formed on the wall, and the angle between the tensile strain bands and the horizontal line is about 45 degrees. In the middle of the wall, it shows x-shaped intersection phenomenon, which is parallel to the angular tensile strain band, but does not extend to the diagonal. When the wall is damaged, an oblique crack is formed from the upper left side to the lower right side, and at the same time, the lower left side and the upper right side both show an oblique crack of 45 degrees. The numerical simulation test specimen fracture development process and fracture distribution pattern are almost exactly the same as the experimental results, except that the numerical simulation shows angular crushing phenomenon while the experiment does not, as shown in Figs.11(g) and 11(h).

The comparison of load-displacement hysteretic curves of each wall in Fig. 12 show that under the action of reciprocating load, the positive ultimate bearing capacity is greater than the reversed ultimate bearing capacity, the main reason for this phenomenon is that the negative ultimate bearing capacity is reduced due to the internal damage of the wall caused by the positive loading. For specimens with mortar strength of 0.4 MPa and 1.0 MPa, when the horizontal displacement at the top of the wall is less than 1 mm, the hysteretic loop shape is relatively narrow, and the material is in the state of linear elasticity. The displacement at the top of the wall is 2–3 mm, reaching the ultimate bearing capacity. The mortar strength of the specimen is 1.0 MPa, the test wall failure is a diagonally through crack and the numerical wall failure is a "> <" crack. Considering the size of the crack, the energy consumed by the diagonally through crack is generally larger than that of the "> <" crack. This helps explain why the hysteresis curve of the numerical simulation is not as full as the test curve. As for the reason why the test wall shows the diagonally through crack, instead of the "> <" crack, the authors are not very certain but the material and construction uncertainties might partly account for deviation.

For the specimen with mortar strength of 2.5 MPa, when the top displacement of the wall reaches 1.4 mm, the bearing capacity of the member decreases rapidly and then shows a stable state, the main reason for this phenomenon is that the load displacement increases too much and the material shows strong brittleness. For specimens with mortar strength of 5.0 MPa, the wall reaches the ultimate bearing capacity when the top displacement is close to 3 mm, and then shows reduced bearing capacity and stiffness degradation. Specimen comparisons show that, as the masonry mortar strength increases, the ultimate bearing capacity of the walls increases gradually. The walls with low strength mortar (mortar strength of 0.4 MPa and 1.0 MPa) have low ultimate bearing capacity and the reciprocating load stiffness degradation rate is slow. For specimens with higher mortar strength (mortar strength of 2.5 MPa and 5.0 MPa), the corresponding ultimate bearing capacity is higher and the stiffness degradation rate is faster.

The comparison results in Fig. 12 show that the hysteretic curve of the numerical model has great similarity with the test data in initial elastic stiffness, ultimate bearing capacity, stiffness degradation characteristics and hysteretic curve shape. The applicability and reliability of the constitutive model are verified.

5 Conclusions

This study aims to better simulate the nonlinear characteristics of masonry materials. The concrete damage model proposed by Faria and Oliver is used as a reference and further improved. The tensile plastic permanent deformation could be now considered. To validate the effectiveness of the proposed model, numerical simulations of the brick masonry under monotonic and cyclic uniaxial tensile and compressive loads were carried out. Simulation of four pieces of masonry walls with different mortar strengths under low cycle reciprocating loadings were conducted.

In this study, the plastic evolution equation was established in the effective stress space. The equations of tensile and compressive yield surfaces of the effective stress were defined by Rankine theory and Drucker-Prager theory, respectively. Meanwhile, the plastic deformation was considered by the method of empirical expression to avoid the complex processing of the softening section. Based on the theory of irreversible thermodynamics, the effective stress tensor was split into two components, and the damage state of the material and mechanical effect of the structure containing the damage was described using the tensile and compressive damage variables. The elastic Helmholtz free energy was defined. Also, the damage criterion was established based on the elastic-plastic damage energy release rate. The evolution law of damage variables was obtained

using the orthogonal law. A double scalar elastic-plastic damage model was established based on the basic principles of thermodynamics. The model presented herein takes into account the strength and stiffness degradation, unilateral effect and hysteresis mechanism, and is implemented by a user-defined material model subroutine in LS-DYNA.

The constitutive model proposed in this study is used to calculate the masonry uniaxial tensile responses. The calculated stress-strain curve obtained reflects the uniaxial tensile failure characteristics of masonry. Before reaching the ultimate tensile strength, the stress-strain curve of masonry shows a complete linear elastic state, after reaching the peak strength, the stress-strain curve shows a rapid downward trend, when the tensile strain reaches 10 times the peak strength corresponding strain, the material tensile strength is almost completely lost. Compared with the test data, the compression stress-strain curve, obtained using the proposed model, shows good consistency at the rising phase. Meanwhile, the simulation results decrease slower but in a more stable way. The two curves intersect at the point $\varepsilon/\varepsilon_m$=3.8, after that, the strength of the material declines rapidly. Compared with the random damage constitutive model proposed by Yang (theoretical formula in Fig. 4), the residual strength of masonry materials in the descending section is overestimated by the model in this study. However, this does not affect the application of the model in the study of seismic performance of masonry structure, because most masonry walls are shear type failure, and few are compression type failure.

Furthermore, the numerical results of uniaxial compression and tensile cyclic loading show that the proposed model can consider the plastic permanent deformation under tensile and compressive loads, and can well reflect the hardening, softening, stiffness degradation characteristics of masonry materials, and the unilateral effect of cyclic loading.

Finally, four masonry walls with different mortar strength are tested and analyzed. The results show that the model has successfully reproduced the main characteristics of the wall failure in the pseudo-static test. Under the action of horizontal reciprocating load, all four pieces of walls show shear type failure while they showed differences at the angle and distribution of the shear fractures. By comparing the load-displacement curves obtained by numerical simulation with the test results, it is found that the model presented herein has satisfactory matching effects in terms of initial elastic stiffness, ultimate bearing capacity, stiffness degradation mechanism and hysteretic curve shape.

The proposed model requires few input parameters, simple calibration, and high computational efficiency. The above numerical analysis results show that it is a suitable and reliable tool to reproduce test results and predict the response of masonry walls under pseudo-static loads. When the proposed model is used to simulate the shear resistance of the wall, the element strain increases with the increase of the horizontal displacement, and large deformation analysis can only be carried out with the help of element failure; otherwise, the element will produce abnormal strain and it is difficult to carry out subsequent analysis.

Acknowledgement

This work is supported by the National Key Research and Development Program of China (2018YFC1504400 and 2019YFC1509301), Natural Science Foundation of China (52078471), and Scientific Research Fund of Institute of Engineering Mechanics, China Earthquake Administration (Grant No. 2019EEEVL0402).

References

Abo-El-Ezz A, Nollet MJ and Nastev M (2013), "Seismic Fragility Assessment of Low-Rise Stone Masonry Buildings," *Earthquake Engineering and Engineering Vibration*, **12**(1): 87–97.

Addessi D, Marfia S and Sacco E (2002), "A Plastic Nonlocal Damage Model," *Computer Methods in Applied Mechanics and Engineering*, **191**(13): 1291–1310.

Addessi D, Marfia S, Sacco E and Toti J (2014), "Modeling Approaches for Masonry Structures," *Open Civ. Eng. J*, **8**(1): 288–300.

Addessi D and Sacco E (2012), "A Multi-Scale Enriched Model for the Analysis of Masonry Panels," *International Journal of Solids and Structures*, **49**(6): 865–880.

Agüera ND, Tomello ME and Frau CD (2016), "Structural Response of Unreinforced Masonry Walls," *Journal of Civil Engineering and Architecture*, **10**: 219–231.

Aref AJ and Dolatshahi KM (2013), "A Three-Dimensional Cyclic Meso-Scale Numerical Procedure for Simulation of Unreinforced Masonry Structures," *Computers and Structures*, **120**(2): 9–23.

Bellis MLD and Addessi D (2011), "A Cosserat Based Multi-Scale Model for Masonry Structures," *International Journal for Multiscale Computational Engineering*, **9**(5): 543–563.

Berto L, Saetta A, Scotta R and Vitaliani R (2002), "An Orthotropic Damage Model for Masonry Structures," *International Journal for Numerical Methods in Engineering*, **55**(2): 127–157.

Bretas EM, Lemos JV and Lourenço PB (2014), "A DEM Based Tool for the Safety Analysis of Masonry Gravity Dams," *Engineering Structures*, **59**(2): 248–260.

Cervera M, Oliver J and Manzoli O (1996), "A Rate-Dependent Isotropic Damage Model for the Seismic Analysis of Concrete Dams," *Earthquake Engineering and Structural Dynamics*, **25**(9): 987–1010.

Faria R, Oliver J and Cervera M (1998), "A Strain-Based Plastic Viscous-Damage Model for Massive Concrete Structures," *International Journal of Solids and Structures*, **35**(14): 1533–1558.

Faria R, Oliver J and Cervera M (2000), "On Isotropic Scalar Damage Models For The Numerical Analysis of Concrete Structures," *CIMNE, Monograph PI198, Barcelona*.

Faria R, Oliver J and Cervera M (2004), "Modeling Material Failure in Concrete Structures Under Cyclic Actions," *Journal of Structural Engineering*, **130**(12): 1997–2005.

Fu Qiushi and Qian Jiang (2018), "Seismic Analysis of Masonry Structures Based on Anisotropic Damage Constitutive Model," *Chinese Journal of Computational Mechanics*, **35**(6): 4–9. (in Chinese)

Galvez F, Giaretton M, Abeling S, *et al.* (2018), "Discrete Element Modeling of a Two Storey Unreinforced Masonry Scaled Model," *16th European Conference on Earthquake Engineering*.

Ge Dongdong, Du Chunbo, Miao Qisong and Chen Xi (2021), "Seismic Collapse Simulation of Existing Masonry Buildings with Different Retrofitting Techniques," *Earthquake Engineering and Engineering Vibration*, **20**(1): 127–139. https://doi.org/10.1007/s11803-021-2010-2.

Gong Maosheng, Zuo Zhanxuan, Sun Jing, He Riteng and Zhao Yinan (2021), "Influence of the Column-to-Beam Flexural Strength Ratio on the Failure Mode of Beam-Column Connections in RC Frames," *Earthquake Engineering and Engineering Vibration*, **20**(2): 441–452. https://doi.org/10.1007/s11803-021-2030-y

Hatzigeorgiou G, Beskos D, *et al*. (2001), "A Simple Concrete Damage Model for Dynamic FEM Application," *International Journal of Computational Engineering Science*, **2**(2): 267–286.

Karapitta L, Mouzakis H and Carydis P (2011), "Explicit Finite-Element Analysis for the In-Plane Cyclic Behavior of Unreinforced Masonry Structures," *Earthquake Engineering and Structural Dynamics*, **40**(2): 175–193.

Lee J and Fenves GL (2001), "A Return-Mapping Algorithm for Plastic-Damage Models: 3-D and Plane Stress Formulation," *International Journal for Numerical Methods in Engineering*, **50**(2): 487–506.

Lemaitre J (2000), *A Course on Damage Mechanics*, Berlin: Springer-Verlag.

Lemos JV (2007), "Discrete Element Modeling of Masonry Structures," *International Journal of Architectural Heritage*, **1**(2): 190–213.

Li Jie and Wu Jianying (2005), "Elastoplastic Damage Constitutive Model for Concrete Based on Damage Energy Release Rates, Part I: Basic Formulations," *China Civil Engineering Journal*, **38**(9): 14–20. (in Chinese)

Li Xiao and Tong Genshu (2021), "Static and Dynamic Inelastic P–Δ Effect for Seismic Design," *Earthquake Engineering and Engineering Vibration*, **20**(3): 645–660. https://doi.org/10.1007/s11803-021-2044-5

Liu Yongbin, Dai Junwu, Yang Yongqiang and Jiang Tao (2020), "Novel Uniaxial Concrete Constitutive Model Considering Bond-Slip Effect," *Earthquake Engineering and Engineering Vibration*, **19**(3): 649–668. https://doi.org/10.1007/s11803-020-0587-5.

Lotfi HR and Shing PB (2016), "Interface Model Applied to Fracture of Masonry Structure," *Journal of Structural Engineering*, **120**(1): 63–80.

Lourenço PB (2009), "Recent Advances in Masonry Modelling: Micromodelling and Homogenisation," *Computational and Experimental Methods in Structures Multiscale Modeling in Solid Mechanics*, pp. 251–294.

Lourenço PB and Rots JG (1997), "Multisurface Interface Model for Analysis of Masonry Structures," *Journal of Engineering Mechanics*, **123**(7): 660–668.

Macorini L and Izzuddin BA (2011), "A Non-Linear Interface Element for 3D Mesoscale Analysis of Brick-Masonry Structures," *International Journal for Numerical Methods in Engineering*, **85**(12): 1584–1608.

Massart TJ, Peerlings RHJ and Geers MGD (2010), "An Enhanced Multi-Scale Approach for Masonry Wall Computations with Localization of Damage," *International Journal for Numerical Methods in Engineering*, **69**(5): 1022–1059.

Oliver J, Cervera M, Oller S and Lubliner J (1990), "Isotropic Damage Models and Smeared Crack Analysis of Concrete," *Proceedings of the Second International Conference on Computer Aided Analysis and Design of Concrete Structures*, Zell am See, pp. 945–957.

Oliveira DV and Lourenço PB (2004), "Implementation and Validation of a Constitutive Model for the Cyclic Behaviour of Interface Elements," *Computers and Structures*, **82**(17): 1451–1461.

Pelà L, Cervera M and Roca P (2011), "Continuum Damage Model for Orthotropic Materials: Application to Masonry," *Computer Methods in Applied Mechanics and Engineering*, **200**(9-12): 917–930.

Petracca M (2016), "Computational Multiscale Analysis of Masonry Structures," *PhD Thesis*, Polytechnic University of Catalonia.

Roca P, Cervera M, Gariup G and Pelà L (2010), "Structural Analysis of Masonry Historical Constructions, Classical and Advanced Approaches," *Arch Comput Methods Eng.*, **17**: 299–325.

Sacco E and Toti J (2010), "Interface Elements for the Analysis of Masonry Structures," *International Journal for Computational Methods in Engineering Science and Mechanics*, **11**: 354–373.

Sachin B Kadam, Yogendra Singh and Li Bing (2020), "Seismic Fragility Reduction of an Unreinforced Masonry School Building Through Retrofit Using Ferrocement Overlay," *Earthquake Engineering and*

Engineering Vibration, **19**(2): 397–412. https://doi.org/10.1007/s11803-020-0569-7

Sarhosis V and Lemos JV (2018), "*A Detailed Micro-Modelling Approach for the Structural Analysis of Masonry Assemblages*," *Computers and Structures*, **206**(AUG.): 66–81.

Schlegel R and Rautenstrauch K (2004), "Numerical Modeling of Discrete Materials-Failure Analysis of Masonry Shear Walls," *Bautechnik*, **80**(7): 15–18.

Shang Qingxue, Guo Xiaodong, Li Quanwang, Xu Zhen, Xie Linlin, Liu Chaofeng, Li Jichao and Wang Tao (2020), "A Benchmark City for Seismic Resilience Assessment," *Earthquake Engineering and Engineering Vibration*, **19**(4): 811–826. https://doi.org/10.1007/s11803-020-0597-3

Simo JC and Ju JW (1987), "Strain- and Stress-Based Continuum Damage Models, I. Formulation," *International Journal of Solids and Structures*, **23**(7): 821–840.

Simo JC and Ju JW (1989), "Strain- and Stress-Based Continuum Damage Models, II. Computational Aspects," *International Journal of Solids and Structures*, **23**(7): 841–869.

Sun Baitao and Zhang Guixin (2018), "Study on Vulnerability Matrices of Masonry Buildings of Mainland of China," *Earthquake Engineering and Engineering Vibration*, **17**(2): 251–259.

Tang Caoming, Luo Rui, Cheng Shaoge and Huang Baodong (2017), "Experimental Study of Seismic Performance of Low Strength Masonry Walls Reinforced with One-Side Cement Mortar Splint," *Journal of Building Structures*, **38**(10): 157–167. (in Chinese)

Toti J, Gattulli V and Sacco E (2015), "Nonlocal Damage Propagation in the Dynamics of Masonry Elements," *Computers and Structures*, **152**(May): 215–227.

Valliappan S, Yazdchi M and Khalili N (1999), "Seismic Analysis of Arch Dams - A Continuum Damage Mechanics Approach," *International Journal for Numerical Methods in Engineering*, **45**(11): 1695–1724.

Wu Jianying, Li Jie and Faria R (2006), "An Energy Release Rate-Based Plastic-Damage Model for Concrete," *International Journal of Solids and Structures*, **43**(3-4): 583–612.

Yang Weizhong Y, Cao Wenwen and Wang Qian (2013), "Research on Stochastic Damage Constitutive Relation of Masonry Subjected to Axial Loading," *Journal of Zhengzhou University* (*Natural Science Edition*), **45**(2): 109–114. (in Chinese)

Yi Weijian and Li Peng (2006), "Experiments Study of Masonry Construction Constitutive Relationship Under Axial Compression," *Sciencepaper Online*, **1**(2). (in Chinese)

Yue Jianguang, Qian Jiang, Wu Kai, *et al.* (2012), "A Modified Plastic Damage Model for Masonry Structure," *Chinese Quarterly of Mechanics*, **33**(1): 146–152. (in Chinese)

Zheng Nina, Li Yingmin and Pan Yi (2011), "Seismic Behavior of Low Masonry Structure with Core-Tie-Columns," *Journal of Southwest Jiaotong University*, **46**(1): 24–29, 55. (in Chinese)